Phosphorylation-dependent inhibition of Cdc42 GEF Gef1 by 14-3-3 protein Rad24 spatially regulates Cdc42 GTPase activity and oscillatory dynamics during cell morphogenesis

Maitreyi Das[a,*], Illyce Nuñez[a], Marbelys Rodriguez[a], David J. Wiley[a], Juan Rodriguez[a], Ali Sarkeshik[b], John R. Yates, III[b], Peter Buchwald[a], and Fulvia Verde[a,c]

[a]Department of Molecular and Cellular Pharmacology, University of Miami Miller School of Medicine, Miami, FL 33101; [b]Department of Chemical Physiology, Scripps Research Institute, La Jolla, CA 92037; [c]Marine Biological Laboratory, Woods Hole, MA 02543.

ABSTRACT **Active Cdc42 GTPase, a key regulator of cell polarity, displays oscillatory dynamics that are anticorrelated at the two cell tips in fission yeast. Anticorrelation suggests competition for active Cdc42 or for its effectors. Here we show how 14-3-3 protein Rad24 associates with Cdc42 guanine exchange factor (GEF) Gef1, limiting Gef1 availability to promote Cdc42 activation. Phosphorylation of Gef1 by conserved NDR kinase Orb6 promotes Gef1 binding to Rad24. Loss of Rad24–Gef1 interaction increases Gef1 protein localization and Cdc42 activation at the cell tips and reduces the anticorrelation of active Cdc42 oscillations. Increased Cdc42 activation promotes precocious bipolar growth activation, bypassing the normal requirement for an intact microtubule cytoskeleton and for microtubule-dependent polarity landmark Tea4-PP1. Further, increased Cdc42 activation by Gef1 widens cell diameter and alters tip curvature, countering the effects of Cdc42 GTPase-activating protein Rga4. The respective levels of Gef1 and Rga4 proteins at the membrane define dynamically the growing area at each cell tip. Our findings show how the 14-3-3 protein Rad24 modulates the availability of Cdc42 GEF Gef1, a homologue of mammalian Cdc42 GEF DNMBP/TUBA, to spatially control Cdc42 GTPase activity and promote cell polarization and cell shape emergence.**

Monitoring Editor
Doug Kellogg
University of California, Santa Cruz

Received: Feb 20, 2015
Revised: Jul 30, 2015
Accepted: Jul 30, 2015

INTRODUCTION

Establishment of cell polarity and maintenance of cell shape are fundamental cellular processes in development and cell differentiation. Defects in cell morphogenesis are linked to diseases such as cancer, developmental defects, and neuronal disorders (Yoshimura *et al.*, 2006; Tanos and Rodriguez-Boulan, 2008; Tahirovic and Bradke, 2009; Carroll and Das, 2011; Yates and Dean, 2011). The conserved GTPase Cdc42 is a key regulator of polarized cell growth (Johnson, 1999; Etienne-Manneville, 2004). Active, GTP-bound Cdc42 promotes asymmetric actin cytoskeleton organization, membrane recycling, and vesicle secretion at the site of polarized cell growth (Pruyne and Bretscher, 2000; Heasman and Ridley, 2008; Harris and Tepass, 2010; Perez and Rincon, 2010; Martin and Arkowitz, 2014). Although substantial progress has been made in our understanding of the cellular processes underpinning cell polarization (Suzuki and Ohno, 2006; Slaughter *et al.*, 2009; Das and Verde, 2013; Wu and Lew, 2013; Halaoui and McCaffrey, 2015), the molecular mechanisms that spatially regulate Cdc42 activity during cell morphogenesis are still poorly understood.

Fission yeast is a particularly amenable model system for studies of cell morphogenesis because it grows in a polarized manner from two cell tips, or cell ends, and displays a well-defined rod shape. Cellular dimensions are uniform and vary little from cell to cell. Cell diameter is maintained at a constant size during cell growth and

This article was published online ahead of print in MBoC in Press (http://www.molbiolcell.org/cgi/doi/10.1091/mbc.E15-02-0095) on August 5, 2015.

*Present address: Department of Biochemistry and Cellular and Molecular Biology, University of Tennessee, Knoxville, TN 37996.

Address correspondence to: Fulvia Verdel (fverde@med.miami.edu).

Abbreviations used: BAR, Bin/amphiphysin/Rvs167; CRIB, Cdc42/Rac interactive binding; FWHM, full-width at half-maximum; GAP, GTPase-activating protein; GEF, guanidine nucleotide exchange factor; GFP, green fluorescent protein; PH, pleckstrin homology; YFP, yellow fluorescent protein.

division (Streiblova and Wolf, 1972), and during the cell cycle, new daughter cells start growth in a monopolar manner from the old end that existed in the previous cell cycle (old-end take off [OETO]; Streiblova and Wolf, 1972; Mitchison and Nurse, 1985). On exit from G1, cells activate bipolar growth from the new end (new-end take off [NETO]) once a critical cell size is reached (Mitchison and Nurse, 1985). Microtubules also play an important role in the activation of bipolar growth by delivering the Tea1–Tea4 scaffold complex, which functions as a polarity landmark, recruiting type 1 phosphatase (PP1) to the cell tips (Martin and Arkowitz, 2014). It is poorly understood how bipolar growth activation is coordinated with cell size and modulated by microtubules and what mechanisms regulate cellular dimensions.

Active Cdc42 displays oscillatory dynamics at the cell tips in fission yeast, revealing the presence of positive and negative feedback controls (Das *et al.*, 2012). Cdc42 oscillatory dynamics has also been observed in other systems (Carlin *et al.*, 2011; Howell *et al.*, 2012; Kuo *et al.*, 2014). In fission yeast cells, oscillations are anticorrelated at the cell tips; when Cdc42 activity is high at one tip, it is lower at the other, indicating competition for active Cdc42 or its regulators (Das *et al.*, 2012). Our findings indicate that Cdc42 dynamics and distribution are governed by a cell-scale system: varying the levels of Cdc42 regulatory factors changes the behavior of the system, altering the symmetry of Cdc42 distribution at the two cell tips. Because Cdc42 is a key determinant of cell growth, the pattern of bipolar growth activation also changes (Das *et al.*, 2012). In particular, Cdc42 dynamics and distribution at the two cell tips are sensitive to the protein level of the Cdc42 guanine nucleotide exchange factor (GEF) Gef1, suggesting that Gef1 availability is limiting under normal conditions.

We previously reported that the conserved nuclear Dbf2-related (NDR) kinase Orb6 has a function in the spatial distribution of active Cdc42 at the cell membrane of fission yeast (Das *et al.*, 2009). Orb6 is part of the NDR/large tumor suppressor (LATS) family of kinases, with conserved functions in the control of morphogenesis and cell proliferation in eukaryotes (Hergovich *et al.*, 2006). NDR kinases have a role in the control of neuronal differentiation (Zallen *et al.*, 2000; Emoto *et al.*, 2004, 2006; Gallegos and Bargmann, 2004; Zinn, 2004) and, in humans, can function as tumor suppressors (Hergovich *et al.*, 2008; Cornils *et al.*, 2011). In fission yeast, Orb6 kinase is required for maintenance of cell polarity (Verde *et al.*, 1995, 1998) and prevention of ectopic activation of Cdc42 GTPase (Das *et al.*, 2009).

Here we show that the NDR kinase Orb6 governs Cdc42 dynamics and distribution by negatively regulating the Cdc42 GEF Gef1. We show that Gef1 is a Bin-amphiphysin-Rvs (BAR) domain–containing GEF that is related to mammalian TUBA/DNMBP, a Cdc42 GEF with a role in kidney cell polarization (Bryant *et al.*, 2010; Zuo *et al.*, 2011). Variations in the TUBA/dynamin-binding protein (DNMBP) gene sequence have been linked to Alzheimer's disease in certain ethnic groups (Kuwano *et al.*, 2006; Bettens *et al.*, 2009). Orb6 kinase phosphorylates Gef1 to generate a 14-3-3–binding site, leading to Gef1 sequestration in the cytoplasm. Consistent with a role for Orb6 kinase in limiting Gef1 availability, loss of Orb6-dependent phosphorylation of Gef1 leads to increasingly symmetrical GTP-Cdc42 distribution at the cell tips and precocious bipolar growth activation, which bypasses the requirement for the microtubule cytoskeleton and the microtubule-dependent landmark Tea4-PP1 phosphatase. Further, loss of Gef1 phosphorylation increases cell width. We find that increasing levels of Cdc42 GTPase-activating protein (GAP) Rga4 can suppress these effects and show that Gef1 and Rga4 cooperate in modulating GTP-Cdc42 distribution. Our findings describe a system that dynamically regulates the shape of Cdc42 distribution at each cell tip, finely scaling up and down the area of cell growth, modulating the extent of cell polarization, and controlling the pattern of cell growth.

RESULTS

Loss of Orb6 kinase activity leads to increased cortical levels of the Cdc42 GEF Gef1 protein

We previously reported that Orb6 kinase spatially regulates Cdc42 GTPase distribution, restricting Cdc42 activation to the cell tips (Das *et al.*, 2009). Decreasing Orb6 kinase activity using an inhibitor-sensitive allele of *orb6*, *orb6-as2*, leads to loss of cell polarity and ectopic activation of Cdc42 at the cell sides that is dependent on the presence of Gef1 (Das *et al.*, 2009). Here we report that loss of Orb6 kinase, in addition to inducing ectopic localization of Gef1 to the cell sides (Figure 1Ad; Das *et al.*, 2009), also strongly increases the cortical levels of Gef1 (Figure 1, Ad and B) compared with controls (Figure 1, A, a–c, and B) within 15 min after addition of the inhibitor 1-Na-PP1 (Figure 1A). Conversely, treatment of wild-type cells with 1-Na-PP1 or *orb6-as2* cells with dimethyl sulfoxide (DMSO) did not change Gef1-3x yellow fluorescent protein (YFP) localization (Figure 1, A, a–c, and B). These observations indicate that Orb6 kinase activity negatively regulates the levels of Gef1 at the cortex.

Gef1 shows structural similarity to mammalian Cdc42 GEF TUBA/DNMBP

Fission yeast has two Cdc42 GEFs, Scd1 (Li *et al.*, 2000) and Gef1 (Coll *et al.*, 2003). Deletion of both GEFs leads to loss of viability, suggesting that they perform overlapping essential functions (Coll *et al.*, 2003). We found that the domain structures of Scd1 and Gef1 display crucial differences. Whereas in most Cdc42 GEFs, a Pleckstrin homology (PH) domain precedes the Dbl homology (DH) domain (Rossman *et al.*, 2003), Gef1 contains a C-terminal BAR domain (Figure 1D) as determined by protein fold recognition software (PHYRE2; Supplemental Figure S1A). Of interest, another *Schizosaccharomyces pombe* Rho GEF, Gef3, has also been found to contain a BAR domain before the DH domain. Gef3 interacts with Rho3 and the septin complex and plays a role in cytokinesis (Muñoz *et al.*, 2014; Wang *et al.*, 2015). Sequence comparison of Gef1 with different species using *EnsemblFungi* indicates that Gef1 is an orthologue of the Cdc42 GEF TUBA/DNMBP found in mammals and nematodes (Salazar *et al.*, 2003; Figure 1D and Supplemental Figure S1B). Similar to Gef1, in the TUBA protein, the DH domain is not preceded by a PH domain but instead is followed by a BAR domain (Figure 1D; Salazar *et al.*, 2003). In mammalian cells, TUBA is believed to perform a specialized role in promoting Cdc42-dependent exocytosis (Bryant *et al.*, 2010; Zuo *et al.*, 2011).

Cortical localization of Gef1 is negatively regulated by association with the 14-3-3 protein Rad24

The different domain structure of Gef1 required structure–function analysis. To analyze the function of the different domains of Gef1, we generated nested deletion mutations in the *gef1* gene (Figure 1D) and analyzed their effect on the localization of the corresponding Gef1-3YFP mutant proteins. Under normal conditions, the full-length Gef1-3YFP displays a discernible but faint localization to the cell tips and cell septum (Figure 1Ea). Deletion of the N-terminal domain (amino acids [aa] 1–314) of the Gef1 protein (*gef1-ΔN-term-3YFP* [aa 315–753]; Figure 1D) leads to complete loss of Gef1 localization from the cell cortex (Figure 1Eb). Consistent with loss of Gef1 function in the control of polarization, deletion of the N-terminal domain of the Gef1 protein leads to increased asymmetry of growth

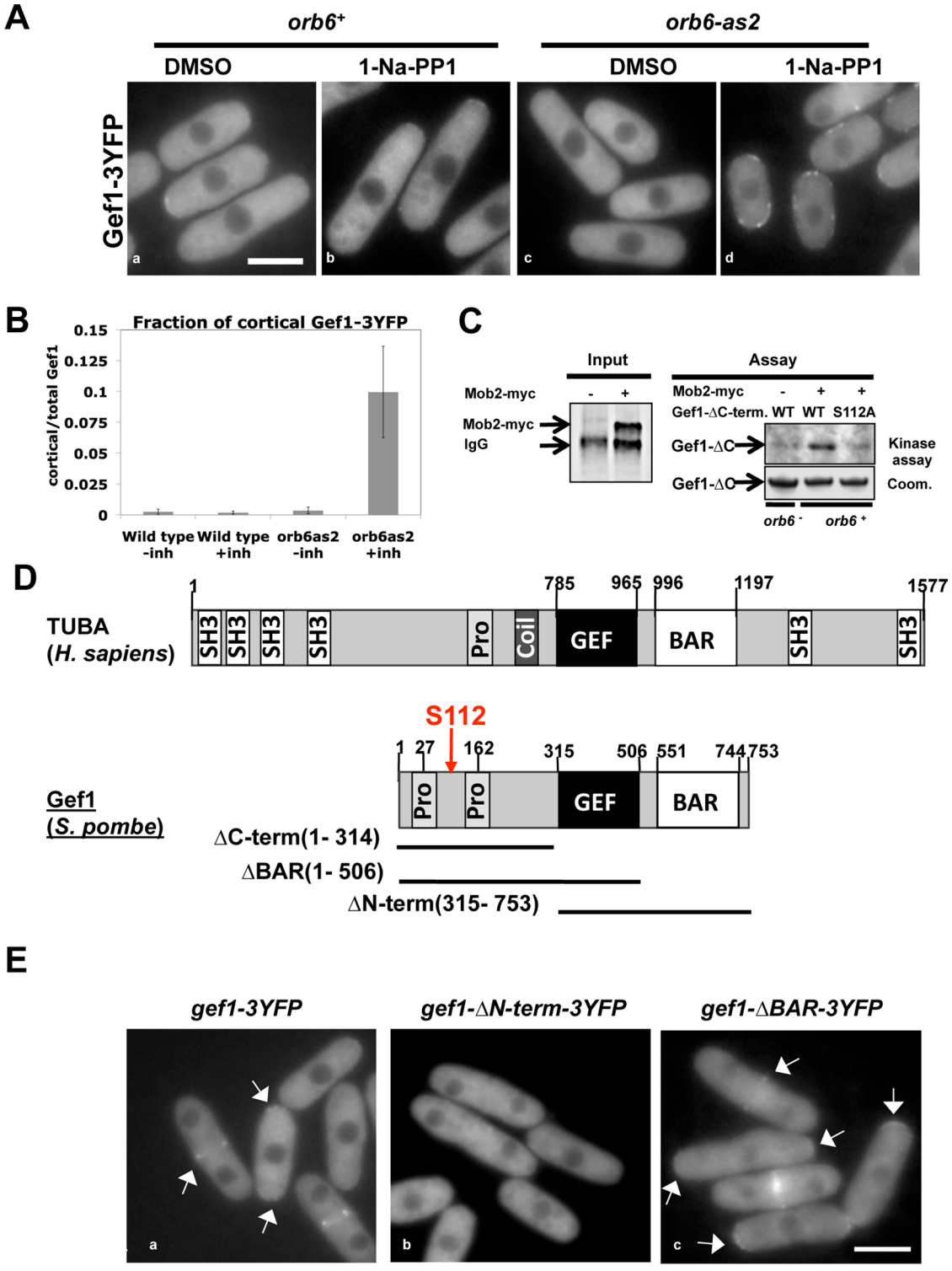

FIGURE 1: Phosphorylation of Gef1 N-terminus by Orb6 kinase. (A) Gef1-3YFP localization in *orb6*$^{+}$ (a, b) and analogue-sensitive *orb6-as2* mutants (c, d) treated with DMSO (a, c) or 50 μM 1-Na-PP1 inhibitor (b, d) for 15 min. Bar, 5 μm. (B) Quantification of the fraction of cells with ectopic Gef1-3YFP localization in control and *orb6-as2* cells in the presence and absence of 50 μM 1-Na-PP1. (C) In vitro phosphorylation of bacterially expressed N-terminal Gef1 (wild type and S112A mutant) by Mob2-bound Orb6 kinase, immunoprecipitated from cell extracts of wild-type and *orb6* mutants (as in Das *et al.*, 2007). (D) Sequence alignment of *S. pombe* Gef1 with human TUBA/DNMBP. Gef1 protein contains a proline-rich Src homology 3 domain (SH3)– binding site at the N-terminus, a GEF domain, and a C-terminus BAR domain. Also shown is a schematic of the deletion mutants of Gef1 analyzed in E. (E) Cortical localization of Gef1 protein (arrows); (a) control Gef1-3YFP, (b) Gef1-ΔNterm-3YFP, and Gef1-ΔBAR-3YFP (c). Bar, 5 μm.

(Supplemental Figure S1C) in which 75% of *gef1-ΔN-term-3YFP* cells are monopolar, similar to *gef1Δ* mutants (71%; see *gef1-3YFP* control cells, 36%). Conversely, deletion of the BAR domain (aa 507–753; *gef1-ΔBAR-3YFP*; Figure 1D) does not affect the localization of Gef1-ΔBAR-3YFP (Figure 1Ec). However, even though the Gef1-BARΔ-3YFP mutant protein is correctly localized to the cell tips and site of cell division, the *gef1-BARΔ-3YFP* mutant cells still display polarization defects (65% monopolar), indicating that the BAR domain is essential for Gef1 function (Supplemental Figure S1C). Protein levels of Gef1-BARΔ-3YFP and Gef1-ΔN-term-3YFP were comparable to full-length Gef1-3YFP in these experimental conditions (Supplemental Figure S1, D and E). Thus our observations indicate that the N-terminal domain (aa 1–314) of Gef1 is essential for its localization to the cell cortex, and the BAR domain is essential for Gef1 function but not localization.

Previous studies with the *Saccharomyces cerevisiae* NDR/Orb6 orthologue, CBK1 kinase, and with mammalian NDR/LATS family kinases identified phosphorylation consensus sequences that are consistent with the pattern Hx[RKH]xx[ST] (Hao *et al.*, 2008; Mazanka *et al.*, 2008). The Gef1 protein has a similar site on its N-terminal region, 107–112 (HRRFFS; Figure 1B, red arrow). Thus we bacterially expressed the N-terminal region of Gef1 (ΔCterm: aa 1–314; Figure 1C) and used this fragment as in vitro substrate for Orb6 kinase immunoprecipitated from yeast cells (Wiley *et al.*, 2003). By mass spectrometry analysis, we determined that a serine residue at position 112 in the N-terminus is directly phosphorylated by Orb6. Consistent with this finding, mutation of the Gef1-S112 to alanine prevents phosphorylation (Figure 1C). We then observed that phosphorylation of serine 112 generates a putative binding site for 14-3-3 proteins. These proteins are highly conserved regulatory proteins that as dimers bind to a wide range of signaling molecules (Hermeking and Benzinger, 2006). They typically interact with ligands with the recognition motif RxxS, where serine is phosphorylated (Yaffe *et al.*, 1997). In *S. pombe*, there are two 14-3-3 proteins, Rad24 and Rad25, which are involved in the DNA damage checkpoint, regulation of transcription, meiosis, and cytokinesis (Kitamura *et al.*, 2001; Ozoe *et al.*, 2002; Mishra *et al.*, 2005; Chen *et al.*, 2008).

A common role of 14-3-3 proteins is sequestration of their targets from the normal site of function (Hermeking and Benzinger, 2006). We hypothesized that Orb6 phosphorylates Gef1 to promote 14-3-3 binding and sequestration of Gef1 in the cytoplasm. We further predicted that loss of 14-3-3 proteins would lead to increased cortical localization of Gef1 and morphological changes. Consistently, we found that with deletion of the 14-3-3 protein, *rad24Δ* mutant cells are wider and rounder (Figure 2Ad) than wild-type cells (Figure 2Aa), whereas cells carrying the deletion of *rad25*, encoding the second 14-3-3 fission yeast protein, do not display a significant change in morphology (Hayles *et al.*, 2013). In *rad24Δ* cells, Gef1-3YFP localization is increased at the cell tips and is often ectopically localized to the cell sides compared with *rad24⁺* control cells (Figure 2, A, b and e, and B). Conversely, the other Cdc42 GEF, Scd1, is normally localized to the cell tips in both *rad24⁺* and *rad24Δ* cells (Figure 2A, c and f). Consistent with a direct physical interaction between Gef1 and Rad24, both Gef1-3YFP protein (Figure 2C) and Gef1-HA protein (Supplemental Figure S2A) from *S. pombe* cell extracts expressing Orb6 kinase copurify with bacterially expressed glutathione *S*-transferase (GST)–Rad24. Further, we found that the interaction of Gef1-3YFP with GST-Rad24 is reduced by inhibition of Orb6-as2 kinase with 1-Na-PP1 (Figure 2D).

Finally, supporting the idea that the morphology defect of *rad24Δ* mutant is mediated by increased Gef1 cortical localization, we found that deletion of the *gef1* gene rescues the altered cell shape of *rad24Δ* cells (Figure 2Ed). The cell diameter of the *gef1Δrad24Δ* double mutant is restored more closely to wild-type cell dimensions than is that of *rad24Δ* cells (Figure 2E and Supplemental Figure S2B). Note that since the *gef1Δrad24Δ* double mutant is not completely restored to wild-type dimensions (Supplemental Figure S2B), it is likely that Rad24 has additional functions in the control of morphogenesis that are not dependent on Gef1.

Overall these findings indicate that Rad24 physically interacts with Gef1 and disruption of the Gef1–Rad24 interaction results in increased cortical localization of Gef1 and ectopic Cdc42 activation.

Loss of Gef1 phosphorylation alters Cdc42 dynamics, leading to increased GTP-Cdc42 symmetry and precocious activation of bipolar growth

Our results suggest that phosphorylation of Gef1S112 mediates Gef1 sequestration to the cytoplasm via an interaction with Rad24. Thus we predicted that loss of phosphorylation at S112 should inhibit the Gef1–Rad24 interaction, resulting in increased cortical localization of Gef1. To test this hypothesis, we substituted serine with alanine at position 112 by site-directed mutagenesis to produce a nonphosphorylatable hemagglutinin (HA)-tagged and 3YFP-tagged form of Gef1 expressed at endogenous levels in a *gef1Δ* mutant. GST-Rad24 pull-down assays indicate that HA-tagged Gef1S112A fails to bind Rad24 protein (Figure 3C). Further, we observed increased cortical localization of Gef1S112A-3YFP compared with wild-type Gef1-3YFP (Figure 3A, a and b). Quantification of Gef1 cortical levels indicated a 10-fold increase of cortical Gef1 in *gef1S112A* (Figure 3B). We did not observe localization of Gef1S112A-3YFP to the cell sides (Figure 3A), suggesting that Rad24 and Orb6 kinase have additional targets that restrict Gef1 localization to the cell tips. Consistent with this idea, Gef1S112A-3YFP localized to the cell sides upon Orb6 kinase inhibition, similar to Gef1-3YFP (Figure 3Dd). On average, the percentage of cells with ectopic localization of Gef1 was similar in *gef1S112A* mutants and *gef1⁺* cells upon Orb6 kinase inhibition (Figure 3E).

We found that the S112A substitution did not change overall protein levels of either Gef1S112A-HA or Gef1-S112A-3YFP compared with Gef1-HA or Gef1-3YFP proteins (Supplemental Figure S3, A and B). To test whether the increased levels of cortical Gef1S112A corresponded to increased activation of Cdc42, we performed a GST–Cdc42/Rac interactive binding (CRIB) pull-down assay (Coll *et al.*, 2003) in *gef1⁺* and *gef1S112A* strains. We found a twofold increase in Cdc42-GTP levels in the *gef1S112A* mutant compared with *gef1⁺* cells (Supplemental Figure S3C).

We then tested the effects of the *gef1S112A* mutation on the distribution of active Cdc42 GTPase, using CRIB–green fluorescent protein (GFP), a fluorescent reporter that binds to GTP-Cdc42 (Tatebe *et al.*, 2008). We previously showed that in small wild-type monopolar cells, the majority of CRIB-GFP is localized at one end, as shown by a heat map of CRIB-GFP tip fractions in cells of various cell sizes (Das *et al.*, 2012; Figure 4B). As the cell grows, CRIB-GFP distribution at the two tips becomes more symmetrical (Das *et al.*, 2012; Figure 4, A and B). Gef1 overexpression leads to increased CRIB-GFP symmetry (Das *et al.*, 2012). Thus we tested whether this effect would also be observable when cortical levels of Gef1 were increased by the *gef1S112A* mutation. Indeed, we found that in *gef1S112A* mutants, even small cells show increased CRIB-GFP symmetry (Figure 4B).

Next we studied GTP-Cdc42 dynamics in control and *gef1S112A* mutants by following CRIB-GFP localization over time. In wild-type cells, active Cdc42 displays oscillatory dynamics, which is anticorrelated at the two cell tips (Das *et al.*, 2012). Anticorrelation of Cdc42

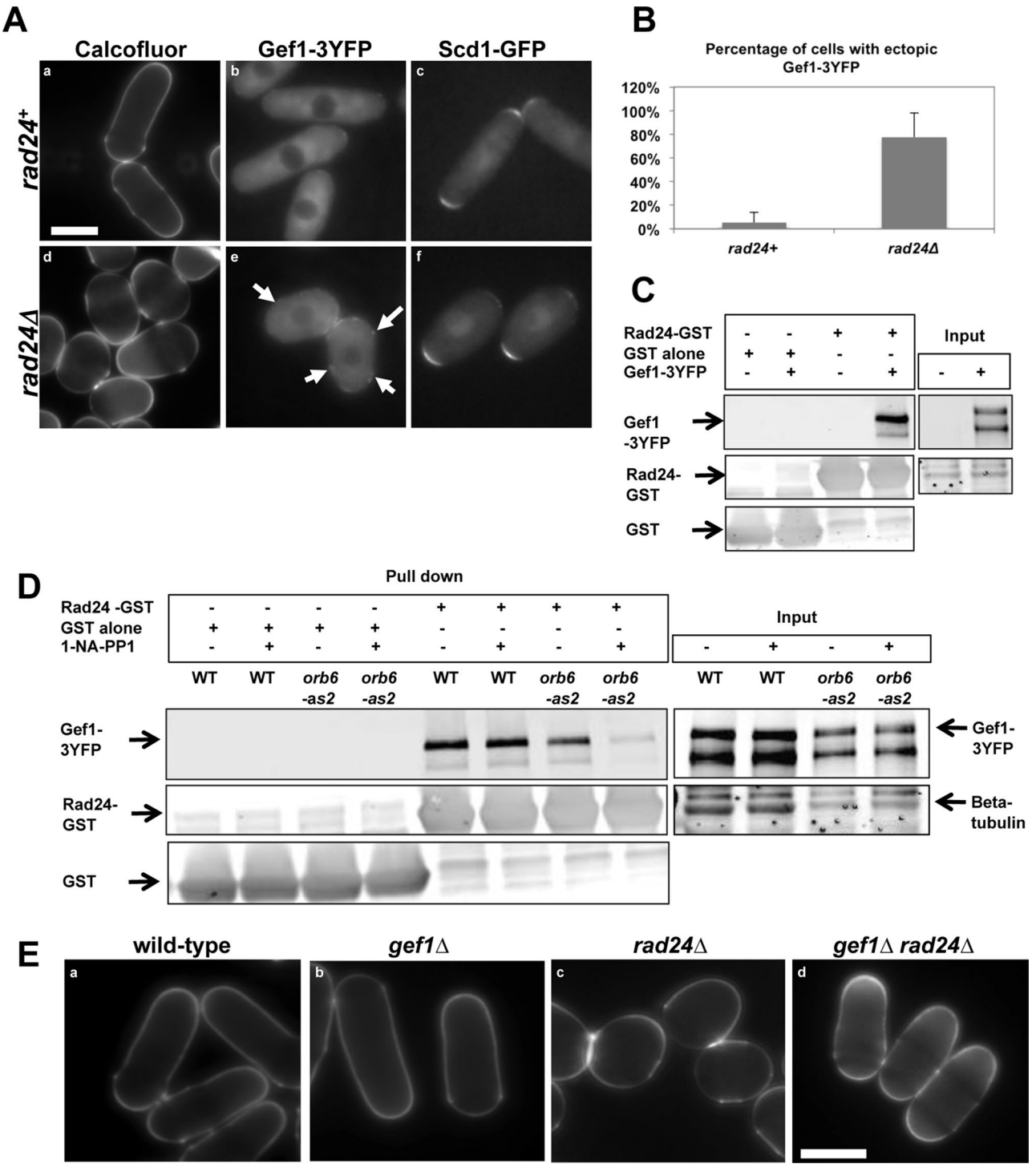

FIGURE 2: The 14-3-3 protein Rad24 physically and functionally interacts with Gef1. (A) *rad24*Δ mutant cells are spherical and show ectopic localization of Gef1-3YFP. Calcofluor staining (a, d), Gef1-3YFP (b, e), and Scd1-GFP (c, f) in control cells (a–c), or *rad24*Δ cells (d–f). Bar, 5 μm. (B) Quantification of the percentage of cells with ectopic Gef1-3YFP localization in wild-type vs. *rad24*Δ cells from the experiment shown in A. (C) Endogenously tagged Gef1-3YFP copurifies with bacterially expressed GST-Rad24 but not with GST alone. (D) Physical interaction between endogenously expressed Gef1-3YFP and bacterially expressed GST-Rad24 is reduced upon inhibition of Orb6-as2 with 50 μM 1-Na-PP1 compared with DMSO treatment (lanes 7 and 8) but remains unchanged in wild-type cells in the presence or absence of the inhibitor (lanes 5 and 6). GST-only control is shown in lanes 1–4. (E) Spherical shape phenotype of *rad24*Δ (c) mutants is rescued in *gef1*Δ*rad24*Δ (d) double-deletion mutants. (a) Control cells; (b) *gef1*Δ cells. Cells were stained with Calcofluor. Bar, 5 μm.

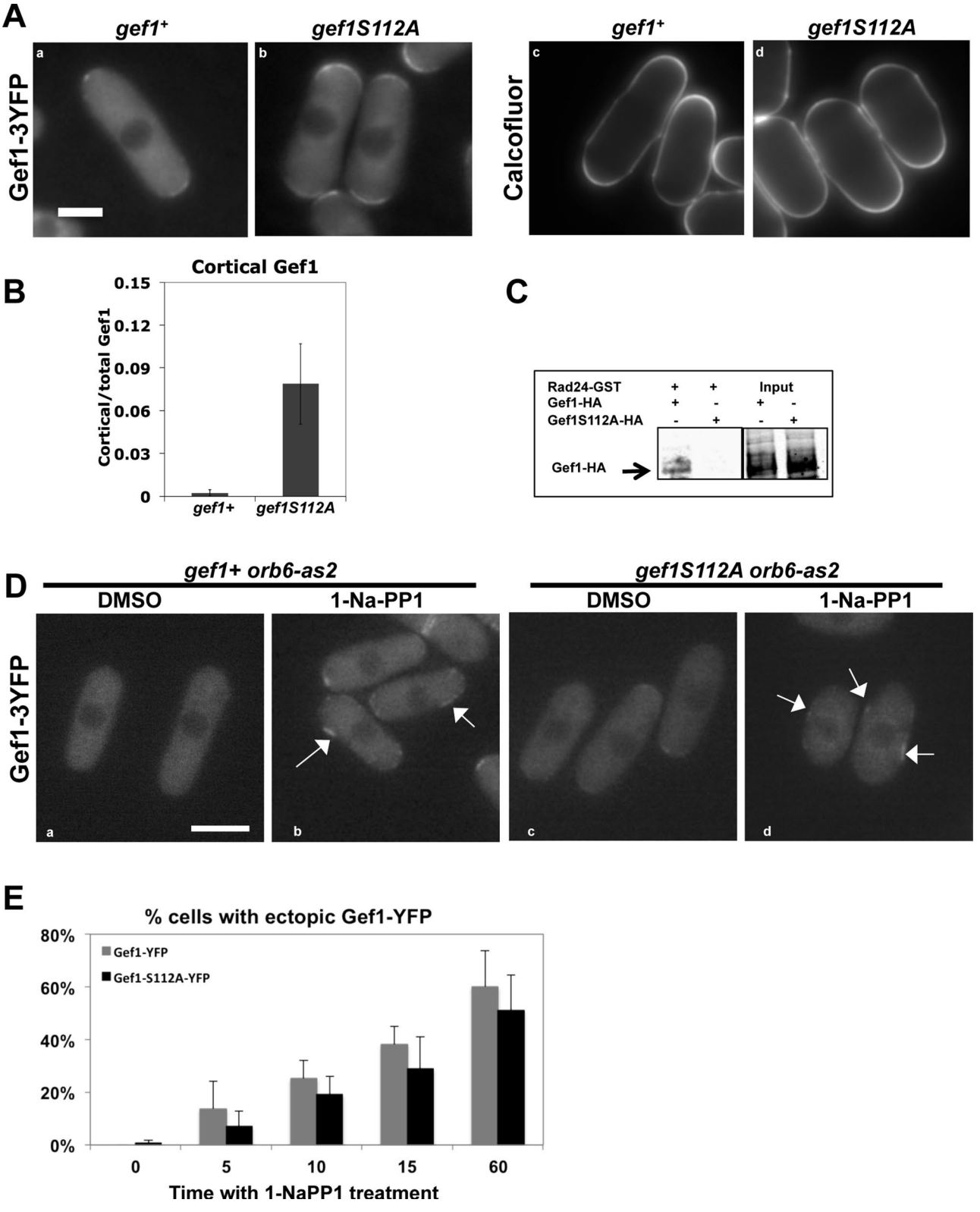

FIGURE 3: Phosphorylation at position S112 in Gef1 regulates Gef1 localization. (A) Cortical localization of Gef1-3YFP increases in *gef1S112A* mutants (a) compared with control *gef1*$^{+}$ cells (b). Calcofluor-stained *gef1S112A* mutant cells (d) show increased cell width compared with control cells (c). Bar, 5 μm. (B) Quantification of Gef1 cortical localization in A. (C) Endogenously tagged Gef1-HA copurifies with bacterially expressed GST-Rad24, whereas Gef1S112A-HA does not. (D) Inhibition of Orb6-as2 kinase with 50 μM 1-Na-PP1 increases cortical localization of both Gef1-3YFP and Gef1S112A-3YFP compared with DMSO treatment. Bar, 10 μm. (E) Quantification of the percentage of cells with ectopic Gef1-3YFP or Gef1S112A-3YFP upon treatment with DMSO (time, 0 min) or 1-Na-PP1 (time, 5, 10, 15, and 60 min).

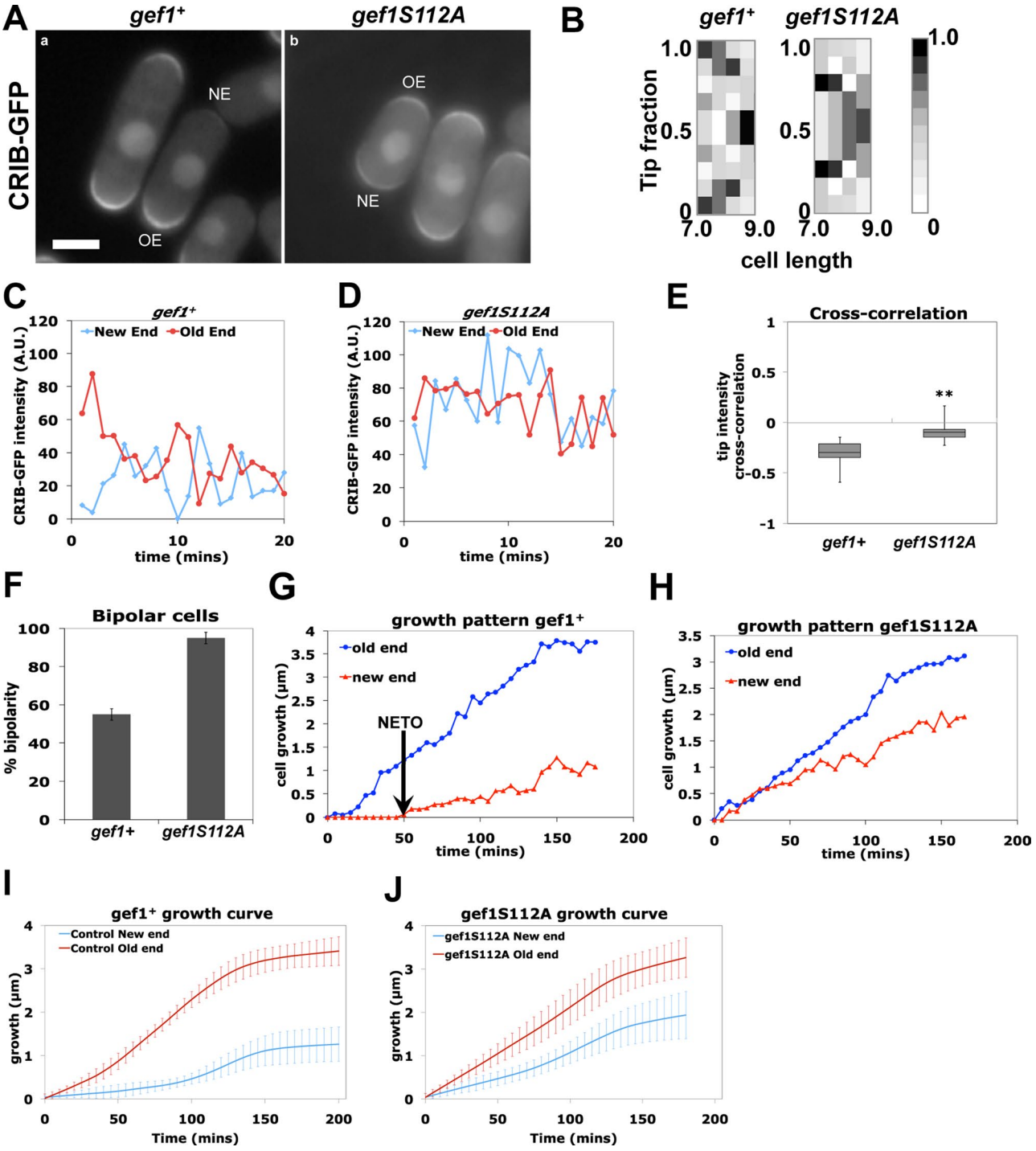

FIGURE 4: Increased cortical Gef1 levels alter Cdc42 dynamics and promote precocious bipolarity. (A) CRIB-GFP is more symmetrically localized at the two tips in *gef1S112A* mutants (b) than in *gef1*$^+$ cells (a); bar, 5 µm. (B) Heat map of CRIB-GFP distribution (tip fraction; Das *et al.*, 2012) in *gef1*$^+$ and *gef1S112A* mutant cells as a function of cell length. (C) Quantification of CRIB-GFP oscillations in control cells expressing Gef1-HA (recorded at 1-min interval). (D) Quantification of CRIB-GFP oscillations in mutant cells expressing Gef1S112A-HA (recorded at 1-min interval). (E) CRIB-GFP cross-correlation at cell tips in Gef1-HA– and Gef1S112A-HA– expressing cells. (F) *gef1S112A* mutant cells show increased bipolarity compared with wild-type cells. Still images of asynchronous Calcofluor-stained cells were analyzed. (G) Cell growth at the old and new ends of a *gef1*$^+$ cell. (H) Cell growth at the old and new ends of a *gef1S112A* mutant cell. Cell growth was recorded and analyzed as previously reported (Das *et al.*, 2007). (I, J) Cumulative growth patterns in *gef1*$^+$ and *gef1S112A* cells, respectively.

oscillations is sensitive to the protein level of Gef1 (Das *et al.*, 2012). Thus we quantified the cross-correlation coefficient of CRIB-GFP oscillations (Figure 4E) in cells expressing Gef1-HA (Figure 4C) and Gef1S112A-HA (Figure 4D) from the endogenous *gef1* promoter. A cross-correlation coefficient of –1 indicates absolute anticorrelation, whereas a cross-correlation coefficient of +1 indicates absolute

correlation. A coefficient value of 0 indicates lack of correlation. As expected, control Gef1-HA cells showed anticorrelation of CRIB-GFP oscillatory dynamics between the two ends (as indicated by a negative cross-correlation coefficient of –0.3 ± 0.13; Figure 4, C and E). However, CRIB-GFP anticorrelation in *gef1S112A-HA* mutants was reduced, approaching the value of 0 (cross-correlation coefficient of –0.08 ± 0.11; Figure 4, D and E). Therefore our results indicate that loss of Gef1 interaction with Rad24 leads to an alteration of Cdc42 dynamics in the cell.

In fission yeast cells, growth occurs from the old end immediately after cell division by a process called OETO (Mitchison and Nurse, 1985). The new end generated as a result of cell division starts growth only when the cell attains a size of at least 9 µm in length by a process called NETO (Mitchison and Nurse, 1985). In *gef1*Δ mutants, NETO is delayed, resulting in an increased percentage of monopolar cells (Coll *et al.*, 2003; Das *et al.*, 2012). We previously proposed that NETO is linked to a progressive alleviation of competition for active Cdc42 (Das *et al.*, 2012). Thus we tested whether increased symmetry of GTP-Cdc42 at the cell tips promotes bipolar growth in *gef1S112A* mutant cells. Indeed, we found that *gef1S112A* mutants display an increased percentage of bipolar cells compared with wild-type cells (Figure 4F). Furthermore, in *gef1S112A* mutants, NETO occurs soon after cell separation, roughly at the same time as OETO (Figure 4, H and J), whereas NETO is delayed in wild-type cells (Figure 4, G and I; Mitchinson and Nurse, 1985). On average, in *gef1S112A* mutants, NETO occurs 7 ± 11.7 min after cell separation, whereas in wild-type cells, NETO occurs 41.5 ± 17.7 min after cell separation ($n = 20$, $p < 0.0001$). Consistent with the idea that NETO occurs precociously and is not due to an alteration of overall cell size, the calculated average cell volume of *gef1S112A* cells undergoing NETO is smaller (76 ± 18.7 µm^3) than that of control *gef1*$^+$ cells undergoing NETO (96 ± 8.4 µm^3; $p < 0.005$). Thus these results indicate that limiting Gef1 localization to the cell tips through a 14-3-3 interaction promotes competition for active Cdc42 and delays the timing of NETO.

Loss of Gef1 phosphorylation suppresses morphological defects associated with microtubule disruption or loss of Tea4-dependent PP1

The microtubule cytoskeleton has an important role in fission yeast cell polarity and the activation of bipolar cell growth (NETO) by delivering the Tea1–Tea4 protein complex, which localizes to the microtubule plus ends and marks the cell tips (Martin and Arkowitz, 2014). The Tea1–Tea4 complex promotes microtubule-induced polarized cell growth in fission yeast by recruiting the type 1 phosphatase Dis2 to the cell tips (Alvarez-Tabares *et al.*, 2007) and promoting Gef1 localization and Cdc42 activation at the site of cell growth by an unknown mechanism (Kokkoris *et al.*, 2014).

Thus we tested the role of Gef1 phosphorylation by Orb6 kinase in the control of microtubule-dependent cell polarization. First, we analyzed the effect of microtubule depolymerization on the distribution of the CRIB-GFP marker. We found that treatment with microtubule inhibitor methyl benzimidazol-2-yl-carbamate (MBC) strongly increases CRIB-GFP asymmetry in *gef1*$^+$ cells (Figure 5A, b and f) compared with DMSO-treated control cells (Figure 5A, a and e). Conversely, *gef1S112A* cells maintain a symmetrical CRIB-GFP distribution after MBC treatment (Figure 5A, d and h), similar to DMSO-treated control *gef1S112A* cells (Figure 5A, c and g), suggesting that loss of Orb6-mediated Gef1 phosphorylation suppresses the effects of microtubule depolymerization.

The microtubule-dependent Tea1–Tea4 complex functions as a targeting subunit for the type 1 phosphatase Dis2 at the cell tips, which has a role in local Gef1 recruitment and Cdc42 activation. Mutant cell cultures carrying the mutation *tea4-V223A* are unable to bind type 1 phosphatase and display decreased levels (30%) of bipolar cells (Supplemental Figure S4; Alvarez-Tabares *et al.*, 2007; Kokkoris *et al.*, 2014), showing monopolar cell growth (Figure 5Bb) and asymmetrical Gef1-3YFP localization (Figure 5Bf). We found that the *gef1S112A* mutation can suppress these phenotypes, promoting localization of Gef1-3YFP at the new end (Figure 5Bh) and bipolar growth activation in *tea4-V223A* cells (66% bipolar cells, similar to control *tea4*$^+$ cells; Figure 5Bd and Supplemental Figure S4, A and B). Collectively our findings indicate that loss of Gef1 phosphorylation by Orb6 kinase rescues the bipolar growth activation defects associated with disruption of the microtubule cytoskeleton and loss of tip-localized type 1 phosphatase.

Orb6-dependent control of Gef1 reveals a scaling relationship in the control of cell diameter

S. pombe cells carrying the *gef1S112A* mutation display altered cellular dimensions (Figures 3Ad and 6A). Indeed, *gef1S112A* mutants display a cell diameter of 4.78 ± 0.2 µm, whereas control *gef1*$^+$ cells display a cell diameter of 3.9 ± 0.2 µm (Figure 6B). To understand how Gef1 availability modulates the maintenance of cell diameter, we studied the functional interaction of Gef1 with other factors involved in diameter control. We found that moderately increasing the levels of Cdc42 GAP Rga4 by inducing its expression from the *nmt1* promoter could fully rescue the wider diameter of *gef1S112A* mutants (3.13 ± 0.2 µm) compared with *gef1S112A* mutant cells alone (4.78 ± 0.2 µm; $p < 0.0001$) and closer to the diameter of control *gef1*$^+$ cells (3.9 ± 0.2 µm; Figure 6, A and B, and Supplemental Figure S5, A and B). Stable induction of the thiamine-repressible *nmt1* promoter was achieved by growth in thiamine-depleted minimal medium for 40 h. We found that *nmt1*-driven *rga4* transcript levels were increased 30-fold over endogenous *rga4* transcript levels (Supplemental Figure S5G), consistent with previous work addressing the strength of the nmt1 promoter (Maundrell, 1990). Conversely, deletion of *rga4* leads to a synthetic phenotype in cells expressing Gef1S112A. *gef1S112A rga4*Δ cells are almost completely round, with a considerably increased cell diameter (6.05 ± 0.4 µm) compared with control cells or *gef1S112A* mutant cells (Figure 6, A and B; $p < 0.0001$).

To gain insight into how Gef1 and Rga4 cortical levels alter cell diameter by modulating the levels of active Cdc42 at each cell tip, we quantified the intensity of CRIB-GFP distribution at the plasma membrane in mutants expressing varying levels of Rga4 and Gef1. In wild-type cells, CRIB-GFP distribution at each tip follows a Gaussian (normal) distribution (Kelly and Nurse, 2011). CRIB-GFP distribution in *gef1S112A* cells also follows a Gaussian curve (Supplemental Figure S5C). We found that mutations altering the respective cortical levels of Gef1 and Rga4 reproducibly yielded Gaussian distributions with different spreads (Supplemental Figure S5D). Different Gaussian curves can be compared using the full-width at half-maximum (FWHM) value, which for Gaussian (normal) distributions is related to the SD σ ($\text{FWHM} = 2(2\cdot\ln 2)^{0.5} \approx 2.36\sigma$; Supplemental Figure S5D; Das *et al.*, 2012). When we plotted the cell diameter as a function of the corresponding FWHM of CRIB-GFP distribution at the cell tips of different mutants (Figure 6D), we found that cell diameter was positively correlated with FWHM in an essentially linear manner (coefficient of determination = 0.988). Cells with a narrower CRIB-GFP distribution (lower FWHM; *gef1*$^+$ *nmt1-rga4* and *gef1S112A nmt1-rga4*) displayed a narrower cell diameter, whereas cells with a wider CRIB-GFP distribution (higher FWHM; (*gef1S112A* and *gef1S112A rga4*Δ) displayed a wider cell diameter (Figure 6D).

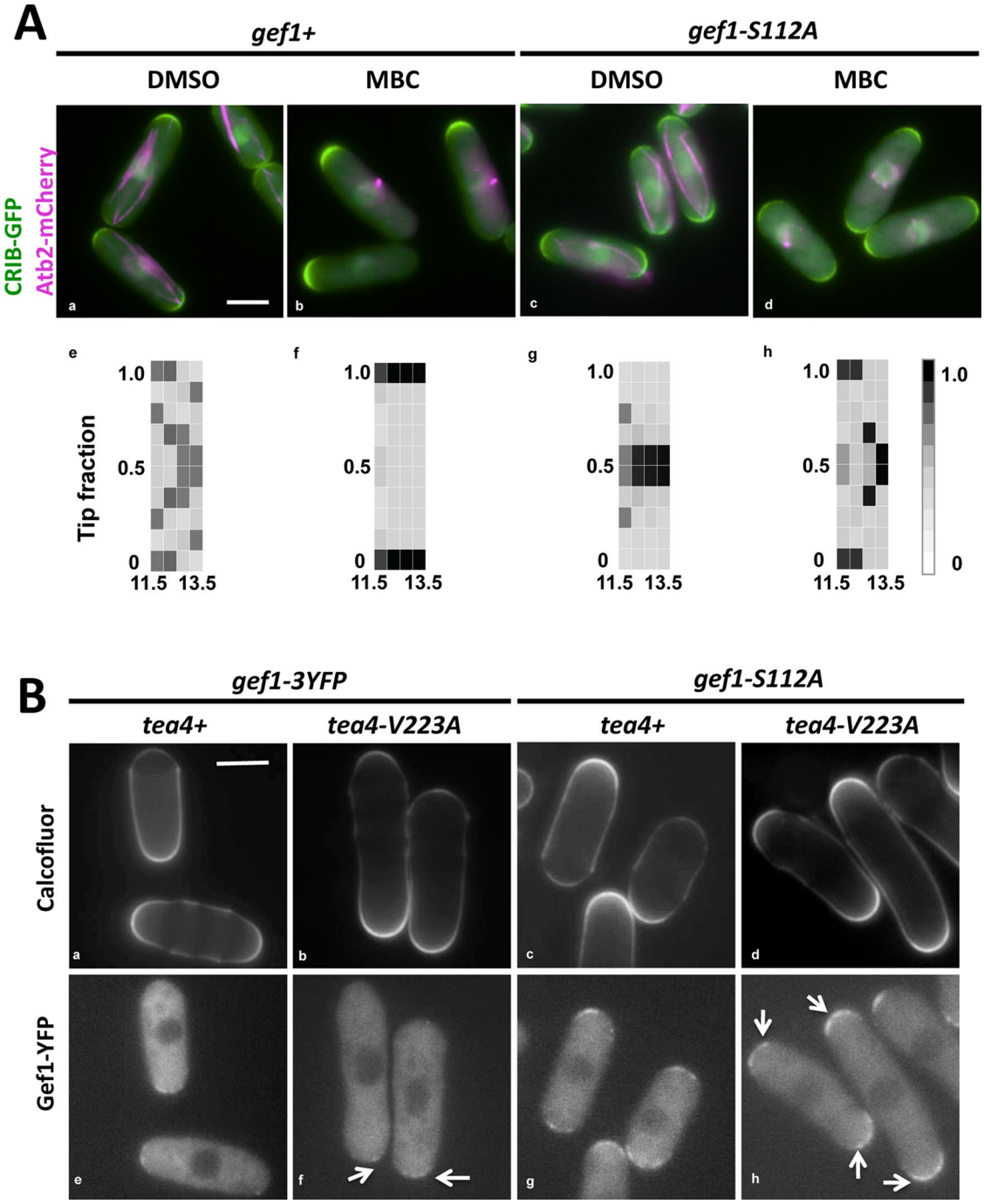

FIGURE 5: Increased cortical Gef1 levels rescue Cdc42 distribution phenotypes associated with disruption of the microtubule cytoskeleton or loss of the Tea4-PP1 polarity landmark. (A) CRIB-GFP asymmetry increases after treatment with microtubule-depolymerizing drug MBC in *gef1*$^{+}$ control cells but not in *gef1S112A* cells. CRIB-GFP and tubulin Atb2-mCherry visualization in *gef1*$^{+}$ cells (a, b) or *gef1S112A* cells (c, d) treated with DMSO (a, c) or microtubule inhibitor MBC (25 µg/ml; b, d) for 45 min at 32°C. Heat map of CRIB-GFP distribution as a function of cell length in cells shown in a–d. Bar, 5 µm. (B) The *gef1S112A* mutation promotes bipolar cell growth in Tea4-V223A–expressing cells. Calcofluor staining (a–d) and Gef1-3YFP localization (e–h) in control Tea4-expressing *tea4*Δ cells (a, e), Tea4-V223A–expressing *tea4*Δ cells (b, f), Tea4-expressing *tea4*Δ *gef1S112A* cells (c, g), and Tea4-V223A–expressing *tea4*Δ *gef1S112A* cells (d, h). Tea4- and Tea4-V223A–expressing *tea4*Δ cells were grown in the absence of thiamine for 18 h at 32°C. Bar, 5 µm.

Cell tip growth at the fission yeast cell tip depends on membrane expansion, mediated by the Cdc42-dependent exocyst function and actin cable assembly (Bendezu and Martin, 2011; Estravis *et al*., 2011). We speculated that establishment of cell diameter is directly dependent on the size of the growth area at the tip. In fission yeast cells, the shape of the growing tip can be quantified by using the Rcurve parameter, the radius of the curvature at the tip (Campas and Mahadevan, 2009;

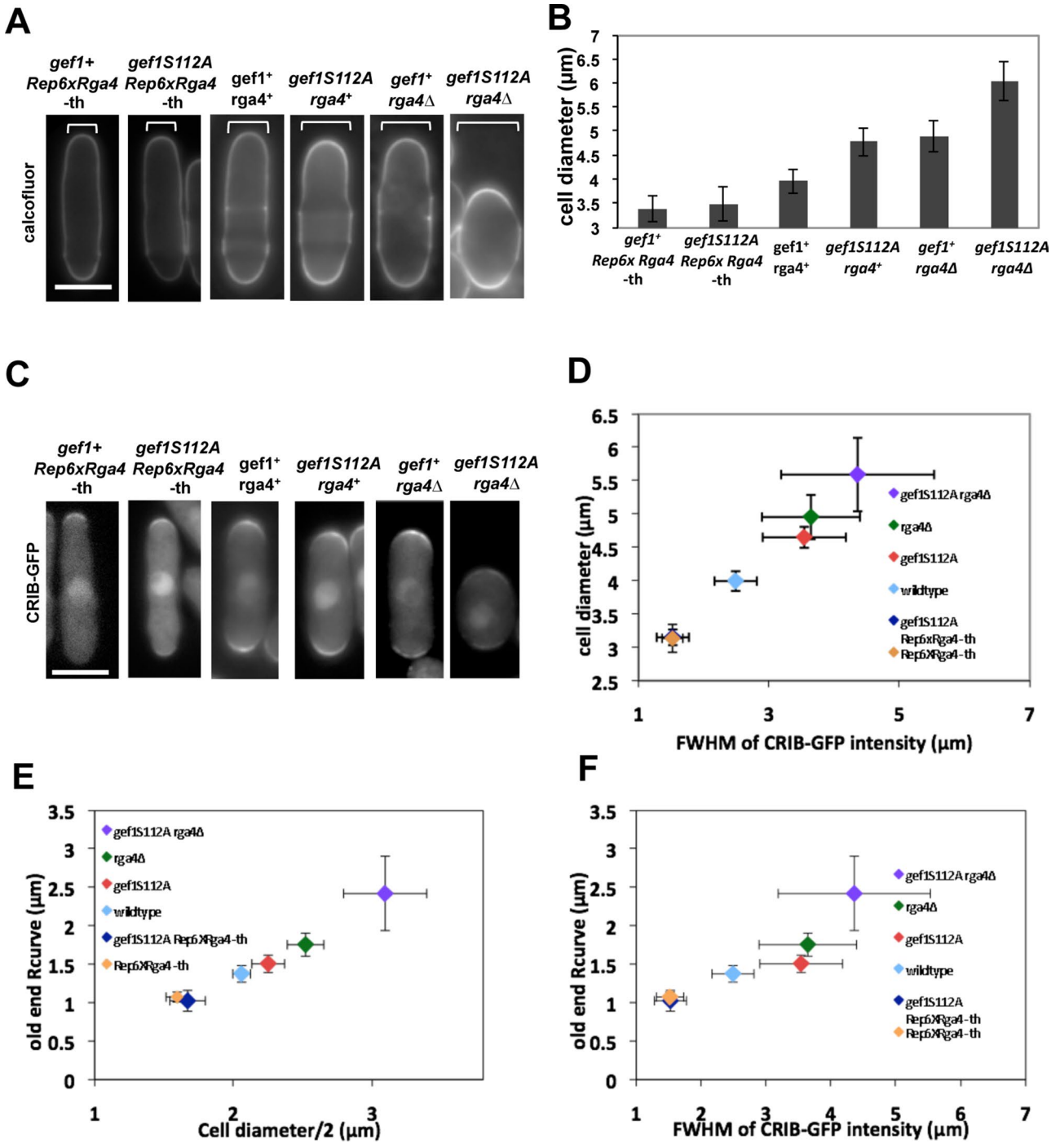

FIGURE 6: Levels of the Cdc42 GEF Gef1 and Cdc42 GAP Rga4 modulate the distribution of active Cdc42 at the cell tips. (A) Fission yeast cell diameter increases with increasing cortical levels of Gef1 and decreasing levels of Rga4. *gef1*$^+$ and *gef1S112A* mutants overexpressing Rga4 show the narrowest cell diameter, whereas *gef1S112A rga4*Δ mutant cells display a wide, almost spherical shape. Bar, 5 mm. (B) Quantification of cell diameter in mutants with varying levels of cortical Gef1 and Rga4. Statistical significance was validated when $p < 0.05$. The p values were determined using analysis of variance with SPSS statistics package 16.0 (IBM, New York, NY), followed by Tamhane's post hoc test. (C) Activated Cdc42 (CRIB-GFP) localization at cell tips is distributed over a larger area in cells with increasing cortical levels of Gef1 and/or decreasing levels of Rga4. *gef1*$^+$ and *gef1S112A* mutants overexpressing Rga4 show narrow CRIB-GFP distribution, whereas in *gef1S112A rga4*Δ mutant cells, CRIB-GFP distribution spreads over to the cell sides. (D) Positive correlation of cell diameter with FWHM of CRIB-GFP Gaussian distribution in mutants with varying levels of Rga4 and cortical Gef1. (E) Linear relationship between tip curvature (Rcurve) and cell diameter among mutants with varying levels of cortical Rga4 and Gef1. Rcurve corresponds to the radius of a circle traced along the curvature of the cell tip (Supplemental Figure S5E). (F) Relationship between tip curvature (Rcurve) and CRIB-GFP FWHM in mutants with varying levels of cortical Rga4 and Gef1.

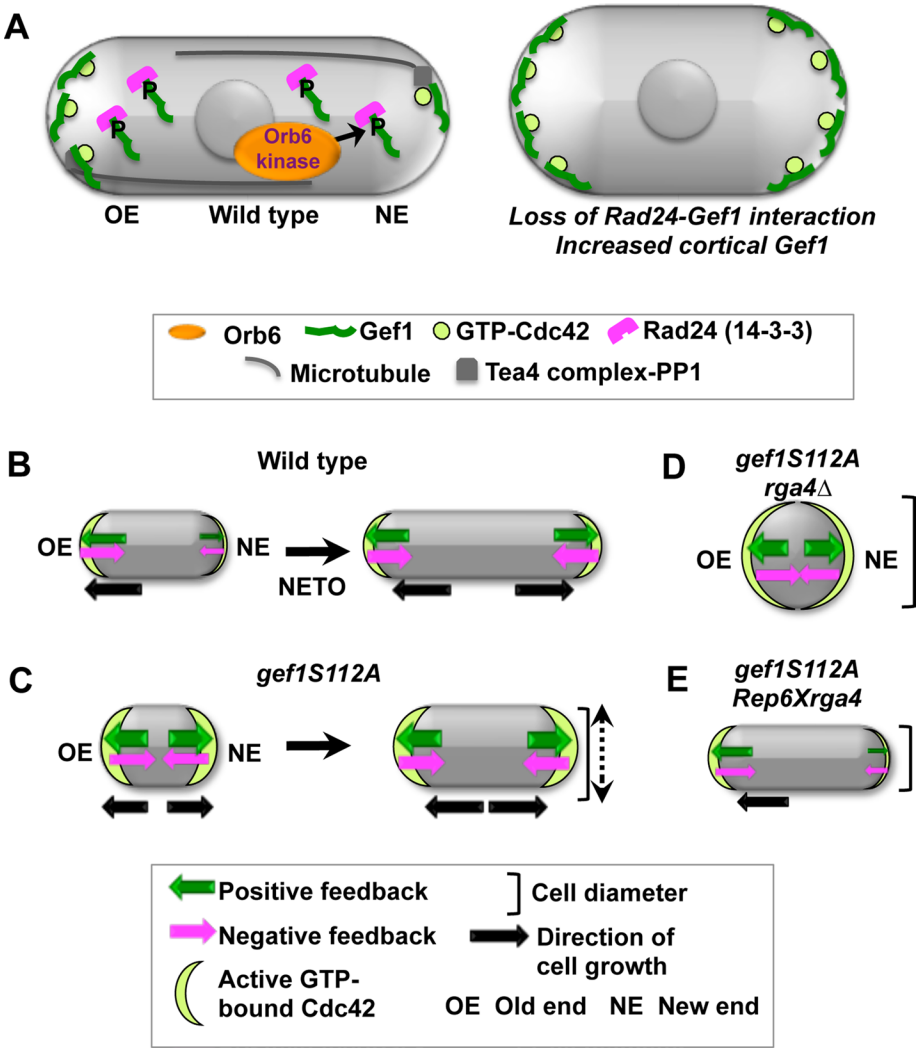

FIGURE 7: Role of Orb6 kinase in the control of Cdc42 oscillatory dynamics, bipolar growth activation, and cell diameter. (A) Left, Orb6 kinase phosphorylates Cdc42 GEF Gef1 to promote Gef1 interaction with 14-3-3 protein Rad24. Gef1 sequestration by Rad24 limits Gef1 cortical levels at the cell tips and thus negatively regulates Cdc42 activation. The microtubule-dependent Tea4-PP1 landmark promotes Gef1 cortical localization and Cdc42 activation. Right, loss of Gef1 interaction with Rad24 leads to increased cortical Gef1 localization and Cdc42 activity, promoting bipolar growth activation irrespective of Tea4-PP1 function. (B–E). Regulation of Cdc42 GTPase activation by Orb6 kinase modulates the size of the area of cell growth and thus cell diameter and temporally controls cell growth in new areas of the cell (new-end take off). (B) Wild-type cells. (C) Increased cortical localization of Gef1 in *gef1S112A* mutants promotes Cdc42 activation, increasing cell width and promoting precocious bipolarity. (D) Loss of Rga4 in *gef1S112A* mutants widens the Gaussian distribution of Cdc42, further widening cell diameter. (E) Overexpression of Rga4 in *gef1S112A* mutants restores normal Cdc42 distribution at the cell tips, reducing cell diameter. The cooperative functions of Gef1 and Rag4 result in a "dynamic border" that controls cell polarization at each tip.

Drake and Vavylonis, 2013; Supplemental Figure S5, E and F). Indeed, in each mutant, we found a tight positive correlation between Rcurve and cell diameter (Figure 6E; coefficient of determination = 0.991), suggesting that the area of active cell growth determines the ultimate size of the cell diameter. Consistent with the idea that the level of Cdc42 activity determines the area of cell tip expansion, we also found a positive correlation between the Rcurve and the FWHM of CRIB-GFP distribution at the growing cell tips (Figure 6F; coefficient of determination = 0.838).

Our observations reveal a cell-scale control mechanism in the regulation of cell polarization and cell morphology. Relative cortical levels of Gef1 and the Cdc42 GAP Rga4 dynamically regulate the Gaussian shape of active Cdc42 distribution, finely scaling up and down the area of cell growth and thus modulating the size of the cell tips, cell diameter, and overall cell proportions. Our findings indicate that by negatively regulating Gef1 function, Orb6 kinase globally affects the pattern of active Cdc42 distribution at the cell membrane, fostering the emergence of cell shape.

DISCUSSION

In this article, we describe a novel molecular mechanism in the control of cell morphology by Cdc42 activation. Our previous studies showed that active Cdc42 displays oscillatory dynamics at the cell tips (Das *et al.*, 2012). Oscillations reveal the presence of positive and negative feedback controls in the system. Anticorrelated Cdc42 oscillations indicate the presence of competition for GTP-Cdc42 and/or its activators, leading to mutually exclusive activation of Cdc42 at the two tips (Das *et al.*, 2012). The control system thus likely consists of Cdc42, Cdc42 regulators, and Cdc42 complex–binding sites on the membrane. Disruption of this control system alters active Cdc42 distribution at a cell-scale level at each tip and cell diameter (Das *et al.*, 2012; Das and Verde, 2013).

Here we deciphered the mechanisms that limit Cdc42 activation by modulating the global level of active Cdc42. We showed previously that cell polarity is maintained through spatial control of active Cdc42 by the conserved NDR kinase Orb6 in a Cdc42 GEF Gef1-dependent manner (Das *et al.*, 2009). Here we showed that Orb6 kinase negatively regulates cortical levels of Gef1, promoting competition for active Cdc42 at the cell tips. Increased active Cdc42 breaks the mutually exclusive activation at the two tips. Consistent with the idea that phosphorylation by Orb6 kinase alters Cdc42 GTPase dynamics, nonphosphorylatable *gef1S112A* mutants with increased cortical localization show decreased Cdc42 asymmetry (Figure 7A) and decreased anticorrelation of GTP-Cdc42 oscillations at the cell tips. Decreased Cdc42 asymmetry in *gef1S112A* mutants alters dependence of bipolar growth activation on a minimal cell size and accelerates the timing of bipolar growth activation (Figure 7C) as compared with wild-type cells (Figure 7B). Thus these findings reveal a mechanism that restrains the extent of global Cdc42 activation.

We show that Gef1 physically interacts with the 14-3-3 protein Rad24 in an Orb6-dependent manner. NDR/Orb6 generates a 14-3-3–binding site on Gef1 through phosphorylation, limiting Gef1

abundance at the tip (Figure 7A). Because *rad24Δ* results in increased cortical localization of Gef1, it is likely that phosphorylated Gef1 can localize to the cell cortex. By binding to phosphorylated Gef1, Rad24 sequestration in the cytoplasm represents one mechanism by which cells limit cortical Gef1 localization to the cell tips. Alternatively, it is also possible that Rad24 functions by displacing Gef1 at the tips. Future studies of Gef1 dynamics at the membrane will address these alternative possibilities. Rad24 was previously reported to be a major regulatory protein in fundamental cellular processes such as checkpoint control, cytokinesis, and transcriptional control (Ford *et al.*, 1994; Forbes *et al.*, 1998; Kitamura *et al.*, 2001; Ozoe *et al.*, 2002; Mishra *et al.*, 2005; Chen *et al.*, 2008). Rad24 also sequesters another *S. pombe* Rho GEF, Rgf1, to prevent its localization to the nucleus, where Rgf1 functions to protect cells against chronic replication stress (Muñoz *et al.*, 2014). Here we describe a novel role for Rad24 in the spatial regulation of Cdc42 GTPase—sequestration of Gef1 to regulate the transition from monopolar to bipolar growth. Phosphorylation of Gef1 by Orb6 indicates that Orb6 behaves similarly to other NDR-type kinases including the LATS family of kinases involved in the control of cell cycle progression and apoptosis (Huang *et al.*, 2005), through the generation of 14-3-3–binding sites (Chen *et al.*, 2008; Hao *et al.*, 2008). Our observations highlight a common modality of substrate regulation among these highly related kinases.

Further, our findings suggest that Orb6, in globally restricting Gef1 availability, has a role in promoting the dependence of Cdc42 activation on the microtubule cytoskeleton (Figure 7A). Microtubules naturally align along the cell main axis, have a role in maintaining the direction of polarized cell growth, and activate the new cell end by delivering the Tea1–Tea4 protein complex to the cell tips (Martin, 2009). Elegant work has shown that microtubules activate Cdc42 by recruiting Gef1 to the cell cortex in a Tea4-bound PP1–dependent manner (Alvarez-Tabares *et al.*, 2007; Kokkoris *et al.*, 2014). Our findings show that *gef1S112A* mutants bypass loss of Tea4-tethered PP1, suggesting a model in which Orb6 functions as a global inhibitor, opposing a microtubule-dependent local activator. Local activation, paired with global inhibition, forms a type of circuitry that is emerging as a unifying principle in cell polarization (Goehring and Grill, 2013). Future experiments will address whether the serine 112 in Gef1 is a direct target of the PP1. Alternatively, other Gef1-binding components (Rincon *et al.*, 2007), Tea4-associated factors (Martin and Arkowitz, 2014), or other phosphatases (Bernal *et al.*, 2012) could also participate in the modulation of Gef1 function.

The *orb6* mutants are round (Verde *et al.*, 1995, 1998), with dynamic CRIB-GFP patches forming throughout the cell cortex (Das *et al.*, 2009). However, *gef1S112A* mutants show increased cell diameter but do not lose polarity. Thus Orb6 kinase likely regulates at least one more Cdc42 regulator in addition to Gef1. The Cdc42 GAP Rga4 is a likely candidate, as it physically (two-hybrid screen) and functionally interacts with Orb6 kinase (Das *et al.*, 2007, 2009). Orb6 kinase possibly regulates both Gef1 and Rga4 to modulate Cdc42 activation, thus controlling cell dimensions and growth symmetry. Future work will address how Orb6 kinase regulates Rga4, which contains several potential Orb6 phosphorylation consensus sites that lie within putative 14-3-3 protein–binding sites.

Rga4 is enriched at the cell sides and was shown previously to have a role in the control of cell diameter (Das *et al.* 2007; Tatebe *et al.*, 2008). In fission yeast, active Cdc42 GTPase distribution at each tip approximates a Gaussian distribution and resembles a gradient (Kelly and Nurse, 2011). Using mutants displaying different cortical levels of Gef1 and Rga4 (Figure 6, D and E), we show that the size of active Cdc42 Gaussian distribution has a positive correlation with cell diameter in a near-linear manner, likely because increasing tip-bound Cdc42 results in growth over a wider area. These observations indicate that distribution of Cdc42 activity is a major determinant of cell tip morphology both in terms of tip curvature (see later discussion) and cell diameter determination. Further, we show that GTP-Cdc42 self-organizes in a Gaussian manner at the cortex, even when the extent of Cdc42 activity varies considerably. Because Gaussian functions are solutions to the continuous diffusion equation, these findings suggest that diffusion-controlled processes regulate active Cdc42 GTPase distributions in all these mutants.

Collectively these observations suggest that the opposing functions of Gef1 and Rga4 continuously modulate the cortical gradient of activated Cdc42, resulting in a "dynamic border" that controls cell polarization at each tip (Figure 7, D and E). This mechanism, in cooperation with other mechanisms of control, such as the negative feedback promoted by the Cdc42- dependent Pak1 kinase, which also limit the extent of Cdc42 activation, promotes Cdc42 oscillatory dynamics (Das *et al.*, 2012). Consistently, *orb6-25* and *pak1/orb2-34* temperature-sensitive mutants display synthetic lethal interactions (Verde *et al.*, 1995, 1998).

Our results reveal another feature of size scaling at the cell tips; we show that increased levels of GTP-Cdc42 lead to cell tips with a wider curvature. Recent theoretical models of cell shape addressed scaling laws in the control of tip morphogenesis. It was proposed that secretion of cell wall material and differential cell wall viscosity modulate tip pointedness, promoting a range of possible cell diameters and tip shapes for which the radius of tip curvature and the radius of the cell body differ (Campas and Mahadevan, 2009; Drake and Vavylonis, 2013). However, we find experimentally that in fission yeast, tip radius and cell diameter are directly proportional upon varying Cdc42 activity, indicating a scaling relationship between tip curvature and cell width. This effect may be due to the dependence of secretion on Cdc42 activity (Estravis *et al.*, 2011), which likely also modulates cell wall maturation via delivery of cell wall biosynthetic enzymes (Estravis *et al.*, 2012). In addition, it is possible that unknown feedback mechanisms, dependent on physical principles such as cell wall viscosity or turgor pressure, may have a role in modulating Cdc42 activity.

Finally, we propose that in fission yeast, by modulating Gef1 availability, the conserved NDR kinase Orb6 establishes the overall scale of cellular dimensions and the number of growing areas. We find that Gef1 is a homologue of the mammalian Cdc42 GEF TUBA/DNMBP, a protein implicated in epithelial cell polarization and associated with late-onset Alzheimer's disease (Kuwano *et al.*, 2006; Bettens *et al.*, 2009; Bryant *et al.*, 2010; Kovacs *et al.*, 2011; Zuo *et al.*, 2011). In mammalian cells, NDR kinases are part of the Hippo tumor suppressor pathway (Hergovich and Hemmings, 2009; Cornils *et al.*, 2011) and have been implicated in neuronal development (Vichalkovski *et al.*, 2008; Emoto, 2011). Because of the conservation of these regulatory modules, it is likely that our findings will have implications for the understanding of cell polarization and other processes in higher eukaryotes.

MATERIALS AND METHODS

Strains and cell culture

S. pombe strains used in this study are listed in Supplemental Table S1. All strains used in this study are isogenic to the original strain 972. Fission yeast cells were cultured in yeast extract (YE) medium or in Edinburgh minimal medium (EMM) plus required supplements. Genetic manipulations and analyses were carried out using standard

techniques (Moreno *et al.*, 1991). Cells were grown exponentially for at least eight generations before analysis.

Microscopy and analysis

Fluorescently tagged cells were microscopically analyzed by an Olympus fluorescence BX61 microscope (Melville, NY) equipped with Nomarski differential interference contrast (DIC) optics, a 100× objective (numerical aperture [NA] 1.35), a Roper CoolSNAP HQ camera (Tucson, AZ), Sutter Lambda 10 + 2 automated excitation and emission filter wheels (Novato, CA), and a 175-W xenon remote source lamp with liquid light guide. Images were acquired and processed using SlideBook image analysis software (Intelligent Imaging Innovations, Denver, CO) and prepared with Photoshop 7 (Adobe, San Jose, CA). Gef1-3YFP cortical localization is sensitive to cell stress. To minimize the effect of stress, cells were imaged for ≤3 min after being mounted on a slide. Gef1-3YFP cortical intensity fraction was analyzed using ImageJ 1.40g software (National Institutes of Health, Bethesda, MD).

The heat map of CRIB-GFP distribution in *gef1*$^+$ and *gef1S112A* mutant cells was generated as follows. The ratio of CRIB-GFP intensity at each cell tip over the total CRIB-GFP intensity (sum of the intensities at both tips) was calculated along with the corresponding cell length. The cells were then binned in cell length groups with 0.5-μm increments. The R software for statistical computing (http://www.r-project.org/) was then used to generate the heat map.

Cell volume was calculated using the formula for a capsule, $3.14r^2(4/3r + a)$, where r is the radius of the cylinder and hemispheres and a is the length of the cylindrical part.

The radius of the curvature at the cell tip, Rcurve, was measured using the ThreePointCircularROI ImageJ plug-in (G. Landini; available at mecourse.com/landinig/software/software.html), which calculates the radius of a circle based on three points selected along the curvature of the cell tip. Three points were chosen at the center of the cell tip and at ~30° left and right of center. Triplicate measurements of the old end were used to avoid tip-shape variability between pre- and post-NETO cells. CRIB-GFP distribution was measured by measuring the intensity of a contour along the cell tip and fitting the average of five measurements to a Gaussian function.

Rad24 binding assays

Bacterially expressed GST, GST-Rad24, was bound to glutathione-linked Sepharose beads or magnetic beads (Pierce, Rockford, IL). The beads were then mixed with fission yeast protein extract from wild-type and Gef1-HA– or Gef1-3YFP–tagged strains incubated overnight at 4°C. To inhibit Orb6 kinase, cells were incubated with either DMSO or 50 μM 1-Na-PP1 (Toronto Research Chemicals, Toronto, Canada) for 15 min at 32°C. The beads were then washed with Tris lysis buffer (50 mM Tris, pH 7.7; 150 mM NaCl; 5 mM EDTA; 5% glycerol; 1% Triton X; 1 mM phenylmethylsulfonyl fluoride; complete EDTA-free protease inhibitor cocktail tablets [Roche Applied Science, Indianapolis, IN]) and separated by SDS–polyacrylamide gel and analyzed by Western blot using mouse monoclonal Anti-HA antibodies (Santa Cruz Biotechnology, Dallas, TX) or anti-GFP (Roche Applied Science).

Construction of Gef1 mutant strains

Gef1 promoter (from position –650 to position –1) was cloned along with the full-length Gef1 gene into of the pFA6-3YFP plasmid. *gef1S112A* mutants were generated by site-directed mutagenesis using a QuikChange Kit (Stratagene, La Jolla, CA). The construct was then transformed into PPG2601 (*gef1::ura4*$^+$ *leu1-32 ura4-D18*) cells, selecting for G418-resistant colonies. The resulting strain contained one functional copy of *gef1S112A* fused to 3YFP followed by *gef1::ura4*$^+$ sequence. Deletion mutants of *gef1* were generated by PCR amplification of different regions of Gef1 open reading frame with the Gef1 promoter (from position –650 to position –1), cloned into the pFA6-3YFP plasmid, and transformed in PPG2601.

In vitro kinase assays and mass spectrometry

Orb6 kinase assay was performed as described in Wiley *et al.* (2003). Myc-tagged Mob2– expressing cells (FV558) and control cells expressing *orb6-as2* mutant were grown in YE to mid log phase at 32°C. Cells were broken using Savant FastPrep FP120 bead beater in HB buffer (25 mm 3-(*N*-morpholino)propanesulfonic acid, pH 7.2, 60 mM β-glycerophosphate, 15 mM *p*-nitrophenyl phosphate, 15 mM $MgCl_2$, 15 mM ethylene glycol tetraacetic acid, 1 mM dithiothreitol, 0.1 M sodium vanadate, 1% Triton X-100, and 1 mM phenylmethylsulfonyl fluoride plus protease inhibitors [complete EDTA-free protease inhibitor cocktail tablets; Roche Applied Science]). Protein G Dynabeads (Invitrogen, Waltham, MA) magnetic beads bound to rabbit anti-Myc antibodies (Santa Cruz Biotechnology) were incubated with (1 mg/ml) protein extracts from *orb6-as2* cells and Myc-tagged Mob2–expressing cells for 1 h and then washed twice with HB buffer and once with kinase buffer (50 mM Tris-HCl, pH 7.5, 100 mM NaCl, 10 mM $MgCl_2$, 1 mM $MnCl_2$). The beads were then resuspended in 25 μl of kinase buffer containing 10 μCi of [γ-^{32}P]ATP (6000 Ci/mmol), 20 μM ATP, and 5 μl of bacterially expressed hexahistidine-tagged N-terminal Gef1. The kinase reaction was incubated for 20 min at 30°C and terminated by added Laemmli buffer, and boiling proteins were then separated on an SDS–polyacrylamide gel.

Mass spectrometry analysis

The in vitro kinase assay was performed with Myc-tagged Mob2–associated Orb6 kinase using bacterially expressed hexahistidine-tagged N-terminal Gef1 as described, with the following exceptions. The samples were split in two; one-half was treated with radioactive [γ-^{32}P]ATP, and the other half was treated with nonradioactive ATP for the kinase assay. The radioactive sample was then loaded on SDS–PAGE gels to detect Gef1 phosphorylation. The nonradioactive sample was trichloroacetic acid (TCA) precipitated as follows. TCA, 100%, was added to the sample to get a final concentration of 20% TCA in ice. The reaction was incubated in ice overnight in a cold room. The reaction was then centrifuged for 30 min at 4°C at 13,000 rpm. The supernatant was discarded by aspiration with only 5–10 μl remaining in the tube. The reaction was then washed with 500 μl of ice-cold acetone twice, with 10-min centrifugation after each wash.

The protein digest was pressure loaded onto a fused-silica 100-μm–inner diameter capillary with a 5-μm pulled tip packed with 10 cm of 3-μm Aqua C18 material (Phenomenex, Ventura, CA) placed inline with an Agilent 1100 quaternary HPLC (Palo Alto, CA). The buffer solutions used were 5% acetonitrile/0.1% formic acid (buffer A) and 80% acetonitrile/0.1% formic acid (buffer B). As peptides eluted from the microcapillary column, they were electrosprayed directly into an LTQ two-dimensional ion trap mass spectrometer (ThermoFinnigan, Palo Alto, CA) with the application of a distal 2.4-kV spray voltage. A cycle of one full-scan mass spectrum (400–1400 *m/z*) followed by eight data-dependent tandem mass spectrometry (MS/MS) spectra at a 35% normalized collision energy was repeated continuously throughout each step of the multidimensional separation. MS scan functions and HPLC solvent gradients were controlled by the Xcalibur data system (Thermo Scientific, Waltham, MA).

Analysis of tandem mass spectra

Tandem mass spectra were analyzed using the following software analysis protocol. Poor-quality spectra were removed from the data set using an automated spectral quality assessment algorithm (Bern *et al.*, 2004). Tandem mass spectra remaining after filtering were searched with the SEQUEST algorithm (Eng *et al.*, 1994) against the *S. pombe* protein sequence database concatenated to a decoy database in which the sequence for each entry in the original database was reversed (Peng *et al.*, 2003). All searches were parallelized and performed on a Beowulf computer cluster consisting of one hundred 1.2-GHz Athlon CPUs (Sadygov, 2002). The MS/MS spectra were searched to consider phosphorylation modifications of +80 on STY. SEQUEST results were assembled and filtered using the DTASelect, version 2.0, program (Tabb *et al.*, 2002; Cociorva *et al.*, 2007). DTASelect 2.0 uses a linear discriminant analysis to dynamically set XCorr and DeltaCN thresholds for the entire data set to achieve a user-specified false-positive rate (5% in this analysis). The false-positive rates are estimated by the program from the number and quality of spectral matches to the decoy database.

ACKNOWLEDGMENTS

We thank Ted Weinert (University of Arizona, Tucson, AZ) and Gennaro D'Urso (University of Miami, Miami, FL) for critical comments on the manuscript; Annie Greene and Leah Nemzow for technical support; Andrew Kim for data analysis; and Seth Schwartz and Chuan Chen for statistical data analysis. We thank Ian Hagan (Cancer Research UK, London, United Kingdom), Kaz Shiozaki (University of California, Davis, Davis, CA), Ken Sawin (University of Edinburgh, Edinburgh, United Kingdom), Pilar Perez (University of Salamanca, Salamanca, Spain), and Mohan Balasubramanian (University of Warwick, Coventry, United Kingdom) for providing strains. Work in F.V.'s laboratory is supported by National Institutes of Health R01 Grant GM095867. Part of this work was also supported by National Science Foundation Grant 0745129. J.R.Y. is supported by National Institutes of Health Grants P41 GM103533 and R01 MH 067880.

REFERENCES

Alvarez-Tabares I, Grallert A, Ortiz JM, Hagan IM (2007). Schizosaccharomyces pombe protein phosphatase 1 in mitosis, endocytosis and a partnership with Wsh3/Tea4 to control polarised growth. J Cell Sci 120, 3589–3601.

Bendezu FO, Martin SG (2011). Actin cables and the exocyst form two independent morphogenesis pathways in the fission yeast. Mol Biol Cell 22, 44–53.

Bern M, Goldberg D, McDonald WH, Yates JR 3rd (2004). Automatic quality assessment of Peptide tandem mass spectra. Bioinformatics 20(Suppl 1), i49–i54.

Bernal M, Sanchez-Romero MA, Salas-Pino S, Daga RR (2012). Regulation of fission yeast morphogenesis by PP2A activator pta2. PLoS One 7, e32823.

Bettens K, Brouwers N, Engelborghs S, De Pooter T, De Deyn PP, Sleegers K, Van Broeckhoven C (2009). DNMBP is genetically associated with Alzheimer dementia in the Belgian population. Neurobiol Aging 30, 2000–2009.

Bryant DM, Datta A, Rodriguez-Fraticelli AE, Peranen J, Martin-Belmonte F, Mostov KE (2010). A molecular network for de novo generation of the apical surface and lumen. Nat Cell Biol 12, 1035–1045.

Campas O, Mahadevan L (2009). Shape and dynamics of tip-growing cells. Curr Biol 19, 2102–2107.

Carlin LM, Evans R, Milewicz H, Fernandes L, Matthews DR, Perani M, Levitt J, Keppler MD, Monypenny J, Coolen T, *et al.* (2011). A targeted siRNA screen identifies regulators of Cdc42 activity at the natural killer cell immunological synapse. Sci Signal 4, ra81.

Carroll TJ, Das A (2011). Planar cell polarity in kidney development and disease. Organogenesis 7, 180–190.

Chen CT, Feoktistova A, Chen JS, Shim YS, Clifford DM, Gould KL, McCollum D (2008). The SIN kinase Sid2 regulates cytoplasmic retention of the S. pombe Cdc14-like phosphatase Clp1. Curr Biol 18, 1594–1599.

Cociorva DL, Tabb D, Yates JR (2007). Validation of tandem mass spectrometry database search results using DTASelect. Curr Protoc Bioinformatics Chapter 13, Unit 13.4.

Coll PM, Trillo Y, Ametzazurra A, Perez P (2003). Gef1p, a new guanine nucleotide exchange factor for Cdc42p, regulates polarity in Schizosaccharomyces pombe. Mol Biol Cell 14, 313–323.

Cornils H, Kohler RS, Hergovich A, Hemmings BA (2011). Downstream of human NDR kinases: impacting on c-myc and p21 protein stability to control cell cycle progression. Cell Cycle 10, 1897–1904.

Das M, Drake T, Wiley DJ, Buchwald P, Vavylonis D, Verde F (2012). Oscillatory dynamics of Cdc42 GTPase in the control of polarized growth. Science 337, 239–243.

Das M, Verde F (2013). Role of Cdc42 dynamics in the control of fission yeast cell polarization. Biochem Soc Trans 41, 1745–1749.

Das M, Wiley DJ, Chen X, Shah K, Verde F (2009). The conserved NDR kinase Orb6 controls polarized cell growth by spatial regulation of the small GTPase Cdc42. Curr Biol 19, 1314–1319.

Das M, Wiley DJ, Medina S, Vincent HA, Larrea M, Oriolo A, Verde F (2007). Regulation of cell diameter, For3p localization, and cell symmetry by fission yeast Rho-GAP Rga4p. Mol Biol Cell 18, 2090–2101.

Drake T, Vavylonis D (2013). Model of fission yeast cell shape driven by membrane-bound growth factors and the cytoskeleton. PLoS Comput Biol 9, e1003287.

Emoto K (2011). The growing role of the Hippo–NDR kinase signalling in neuronal development and disease. J Biochem 150, 133–141.

Emoto K, He Y, Ye B, Grueber WB, Adler PN, Jan LY, Jan Y-N (2004). Control of dendritic branching and tiling by the Tricornered-kinase/Furry signaling pathway in Drosophila sensory neurons. Cell 119, 245–256.

Emoto K, Parrish JZ, Jan LY, Jan Y-N (2006). The tumour suppressor Hippo acts with the NDR kinases in dendritic tiling and maintenance. Nature 443, 210–213.

Eng J, McCormack A, Yates J (1994). An approach to correlate tandem mass spectral data of peptides with amino acid sequences in a protein database. J Am Soc Mass Spectrom 5, 976–989.

Estravis M, Rincon S, Perez P (2012). Cdc42 regulation of polarized traffic in fission yeast. Commun Integr Biol 5, 370–373.

Estravis M, Rincon SA, Santos B, Perez P (2011). Cdc42 regulates multiple membrane traffic events in fission yeast. Traffic 12, 1744–1758.

Etienne-Manneville S (2004). Cdc42—the centre of polarity. J Cell Sci 117, 1291–1300.

Forbes KC, Humphrey T, Enoch T (1998). Suppressors of cdc25p overexpression identify two pathways that influence the G2/M checkpoint in fission yeast. Genetics 150, 1361–1375.

Ford JC, al-Khodairy F, Fotou E, Sheldrick KS, Griffiths DJ, Carr AM (1994). 14-3-3 protein homologs required for the DNA damage checkpoint in fission yeast. Science 265, 533–535.

Gallegos ME, Bargmann CI (2004). Mechanosensory neurite termination and tiling depend on SAX-2 and the SAX-1 kinase. Neuron 44, 239–249.

Goehring NW, Grill SW (2013). Cell polarity: mechanochemical patterning. Trends Cell Biol 23, 72–80.

Halaoui R, McCaffrey L (2015). Rewiring cell polarity signaling in cancer. Oncogene 34, 939–950.

Hao Y, Chun A, Cheung K, Rashidi B, Yang X (2008). Tumor suppressor LATS1 is a negative regulator of oncogene YAP. J Biol Chem 283, 5496–5509.

Harris KP, Tepass U (2010). Cdc42 and vesicle trafficking in polarized cells. Traffic 11, 1272–1279.

Hayles J, Wood V, Jeffery L, Hoe KL, Kim DU, Park HO, Salas-Pino S, Heichinger C, Nurse P (2013). A genome-wide resource of cell cycle and cell shape genes of fission yeast. Open Biol 3, 130053.

Heasman SJ, Ridley AJ (2008). Mammalian Rho GTPases: new insights into their functions from in vivo studies. Nat Rev Mol Cell Biol 9, 690–701.

Hergovich A, Cornils H, Hemmings BA (2008). Mammalian NDR protein kinases: from regulation to a role in centrosome duplication. Biochim Biophys Acta 1784, 3–15.

Hergovich A, Hemmings BA (2009). Mammalian NDR/LATS protein kinases in hippo tumor suppressor signaling. Biofactors 35, 338–345.

Hergovich A, Stegert MR, Schmitz D, Hemmings BA (2006). NDR kinases regulate essential cell processes from yeast to humans. Nat Rev Mol Cell Biol 7, 253–264.

Hermeking H, Benzinger A (2006). 14-3-3 proteins in cell cycle regulation. Semin Cancer Biol 16, 183–192.
Howell AS, Jin M, Wu CF, Zyla TR, Elston TC, Lew DJ (2012). Negative feedback enhances robustness in the yeast polarity establishment circuit. Cell 149, 322–333.
Huang J, Wu S, Barrera J, Matthews K, Pan D (2005). The Hippo signaling pathway coordinately regulates cell proliferation and apoptosis by inactivating Yorkie, the Drosophila homolog of YAP. Cell 122, 421–434.
Johnson DI (1999). Cdc42: An essential Rho-type GTPase controlling eukaryotic cell polarity. Microbiol Mol Biol Rev 63, 54–105.
Kelly FD, Nurse P (2011). Spatial control of Cdc42 activation determines cell width in fission yeast. Mol Biol Cell 22, 3801–3811.
Kitamura K, Katayama S, Dhut S, Sato M, Watanabe Y, Yamamoto M, Toda T (2001). Phosphorylation of Mei2 and Ste11 by Pat1 kinase inhibits sexual differentiation via ubiquitin proteolysis and 14-3-3 protein in fission yeast. Dev Cell 1, 389–399.
Kokkoris K, Gallo Castro D, Martin SG (2014). The Tea4-PP1 landmark promotes local growth by dual Cdc42 GEF recruitment and GAP exclusion. J Cell Sci 127, 2005–2016.
Kovacs EM, Verma S, Thomas SG, Yap AS (2011). Tuba and N-WASP function cooperatively to position the central lumen during epithelial cyst morphogenesis. Cell Adh Migr 5, 344–350.
Kuo CC, Savage NS, Chen H, Wu CF, Zyla TR, Lew DJ (2014). Inhibitory GEF phosphorylation provides negative feedback in the yeast polarity circuit. Curr Biol 24, 753–759.
Kuwano R, Miyashita A, Arai H, Asada T, Imagawa M, Shoji M, Higuchi S, Urakami K, Kakita A, Takahashi H, *et al*. (2006). Dynamin-binding protein gene on chromosome 10q is associated with late-onset Alzheimer's disease. Hum Mol Genet 15, 2170–2182.
Li YC, Chen CR, Chang EC (2000). Fission yeast Ras1 effector Scd1 interacts with the spindle and affects its proper formation. Genetics 156, 995–1004.
Martin SG (2009). Microtubule-dependent cell morphogenesis in the fission yeast. Trends Cell Biol 19, 447–454.
Martin SG, Arkowitz RA (2014). Cell polarization in budding and fission yeasts. FEMS Microbiol Rev 38, 228–253.
Maundrell K (1990). nmt1 of fission yeast: a highly transcribed gene completely repressed by thiamine. J Biol Chem 265, 10857–10864.
Mazanka E, Alexander J, Yeh BJ, Charoenpong P, Lowery DM, Yaffe M, Weiss EL (2008). The NDR/LATS family kinase Cbk1 directly controls transcriptional asymmetry. PLoS Biol 6, e203.
Mishra M, Karagiannis J, Sevugan M, Singh P, Balasubramanian MK (2005). The 14–3-3 protein rad24p modulates function of the cdc14p family phosphatase clp1p/flp1p in fission yeast. Curr Biol 15, 1376–1383.
Mitchison JM, Nurse P (1985). Growth in cell length in the fission yeast Schizosaccharomyces pombe. J Cell Sci 75, 357–376.
Moreno S, Klar A, Nurse P (1991). Molecular genetic analysis of fission yeast Schizosaccharomyces pombe. Methods Enzymol 194, 795–823.
Muñoz S, Manjón E, Sánchez Y (2014). The putative exchange factor Gef3p interacts with Rho3p GTPase and the septin ring during cytokinesis in fission yeast. J Biol Chem 289, 21995–22007.
Ozoe F, Kurokawa R, Kobayashi Y, Jeong HT, Tanaka K, Sen K, Nakagawa T, Matsuda H, Kawamukai M (2002). The 14-3-3 proteins Rad24 and Rad25 negatively regulate Byr2 by affecting its localization in Schizosaccharomyces pombe. Mol Cell Biol 22, 7105–7119.
Peng J, Elias JE, Thoreen CC, Licklider LJ, Gygi SP (2003). Evaluation of multidimensional chromatography coupled with tandem mass spectrometry (LC/LC-MS/MS) for large-scale protein analysis: the yeast proteome. J Proteome Res 2, 43–50.
Perez P, Rincon SA (2010). Rho GTPases: regulation of cell polarity and growth in yeasts. Biochem J 426, 243–253.
Pruyne D, Bretscher A (2000). Polarization of cell growth in yeast. I. Establishment and maintenance of polarity states. J Cell Sci 113, 365–375.
Rincon S, Coll PM, Perez P (2007). Spatial regulation of Cdc42 during cytokinesis. Cell Cycle 6, 1687–1691.
Rossman KL, Cheng L, Mahon GM, Rojas RJ, Snyder JT, Whitehead IP, Sondek J (2003). Multifunctional roles for the PH domain of Dbs in regulating Rho GTPase activation. J Biol Chem 278, 18393–18400.
Sadygov RG, Eng J, Durr E, Saraf A, McDonald H, MacCoss MJ, Yates JR III (2002). Code developments to improve the efficiency of automated MS/MS spectra interpretation. J Proteome Res 2, 211–215.
Salazar MA, Kwiatkowski AV, Pellegrini L, Cestra G, Butler MH, Rossman KL, Serna DM, Sondek J, Gertler FB, De Camilli P (2003). Tuba, a novel protein containing bin/amphiphysin/Rvs and Dbl homology domains, links dynamin to regulation of the actin cytoskeleton. J Biol Chem 278, 49031–49043.
Slaughter BD, Smith SE, Li R (2009). Symmetry breaking in the life cycle of the budding yeast. Cold Spring Harbor Perspect Biol 1, a003384.
Streiblova E, Wolf A (1972). Cell wall growth during the cell cycle of Schizosaccharomyces pombe. Z Allg Mikrobiol 12, 673–684.
Suzuki A, Ohno S (2006). The PAR-aPKC system: lessons in polarity. J Cell Sci 119, 979–987.
Tabb DL, McDonald WH, Yates JR 3rd (2002). DTASelect and Contrast: tools for assembling and comparing protein identifications from shotgun proteomics. J Proteome Res 1, 21–26.
Tahirovic S, Bradke F (2009). Neuronal polarity. Cold Spring Harb Perspect Biol 1, a001644.
Tanos B, Rodriguez-Boulan E (2008). The epithelial polarity program: machineries involved and their hijacking by cancer. Oncogene 27, 6939–6957.
Tatebe H, Nakano K, Maximo R, Shiozaki K (2008). Pom1 DYRK regulates localization of the Rga4 GAP to ensure bipolar activation of Cdc42 in fission yeast. Curr Biol 18, 322–330.
Verde F, Mata J, Nurse P (1995). Fission yeast cell morphogenesis: identification of new genes and analysis of their role during the cell cycle. J Cell Biol 131, 1529–1538.
Verde F, Wiley DJ, Nurse P (1998). Fission yeast orb6, a ser/thr protein kinase related to mammalian rho kinase and myotonic dystrophy kinase, is required for maintenance of cell polarity and coordinates cell morphogenesis with the cell cycle. Proc Natl Acad Sci USA 95, 7526–7531.
Vichalkovski A, Gresko E, Cornils H, Hergovich A, Schmitz D, Hemmings BA (2008). NDR kinase is activated by RASSF1A/MST1 in response to Fas receptor stimulation and promotes apoptosis. Curr Biol 18, 1889–1895.
Wang N, Wang M, Zhu YH, Grosel TW1, Sun D1, Kudryashov DS2, Wu JQ (2015). The Rho-GEF Gef3 interacts with the septin complex and activates the GTPase Rho4 during fission yeast cytokinesis. Mol Biol Cell 26, 238–55.
Wiley DJ, Marcus S, D'Urso G, Verde F (2003). Control of cell polarity in fission yeast by association of Orb6p kinase with the highly conserved protein methyltransferase Skb1p. J Biol Chem 278, 25256–25263.
Wu CF, Lew DJ (2013). Beyond symmetry-breaking: competition and negative feedback in GTPase regulation. Trends Cell Biol 23, 476–483.
Yaffe MB, Rittinger K, Volinia S, Caron PR, Aitken A, Leffers H, Gamblin SJ, Smerdon SJ, Cantley LC (1997). The structural basis for 14-3-3:phosphopeptide binding specificity. Cell 91, 961–971.
Yates LL, Dean CH (2011). Planar polarity: a new player in both lung development and disease. Organogenesis 7, 209–216.
Yoshimura T, Arimura N, Kaibuchi K (2006). Molecular mechanisms of axon specification and neuronal disorders. Ann NY Acad Sci 1086, 116–125.
Zallen JA, Peckol EL, Tobin DM, Bargmann CI (2000). Neuronal cell shape and neurite initiation are regulated by the Ndr kinase SAX-1, a member of the Orb6/COT-1/warts serine/threonine kinase family. Mol Biol Cell 11, 3177–3190.
Zinn K (2004). Dendritic tiling; new insights from genetics. Neuron 44, 211–213.
Zuo X, Fogelgren B, Lipschutz JH (2011). The small GTPase Cdc42 is necessary for primary ciliogenesis in renal tubular epithelial cells. J Biol Chem 286, 22469–22477.